Front. Earth Sci. 2025, 19(1): 13–24
https://doi.org/10.1007/s11707-021-0914-9

RESEARCH ARTICLE

Summer phytoplankton blooms off the Somali coast in the South-western Arabian Sea from remote sensing observations

Ying CHEN[1,3*], Ruixue CAO[1,4*], Yuting FENG[1,3], Hui ZHAO (✉)[1,2,3]

1 Guangdong Ocean University, Zhanjiang 524088, China
2 Southern Marine Science and Engineering Guangdong Laboratory, Zhuhai 519080, China
3 Southern Marine Science and Engineering Guangdong Laboratory, Zhanjiang 524088, China
4 Key Laboratory of Climate, Resources and Environment in Continental Shelf Sea and Deep Sea of Department of Education of Guangdong Province, Guangdong Ocean University, Zhanjiang 524088, China

Abstract Summer phytoplankton blooms appear frequently off the Somali coast in the southwestern Arabian Sea (AS), where strong reversal monsoon and summer upwelling is prevailing. Distinct high chlorophyll-a (Chl-*a*) concentrations in summer were displayed in the western AS, especially in the region off the Somali coast. The spatial and inter-annual variations of the summer high Chl-*a* were studied using satellite data including ocean color and wind vectors. Under ocean conditions including monsoon winds, Ekman transport (ET) and Ekman pumping velocity (EPV), as well as geostrophic current and aerosol precipitation, the possible mechanisms of high Chl-*a* was investigated. The summer high Chl-*a* presented strong inter-annual variations in the southwestern AS. The results of simple correlation analysis indicated that there were good correlations between the ET and Chl-*a*, as well as between EPV and Chl-*a*. These implied that the ET and EPV may cause uplift of nutrients into the upper layer of the western AS from subsurface or coastal regions, inducing high Chl-*a* in the southwestern AS, especially in the region off the Somali coasts in summer. The multiple/partial correlation analysis implied further that EPV-induced upwelling may be more helpful than the ET-induced upwelling in the coastal region off Somalia, leading to probably more significant influence of EPV upwelling on the phytoplankton bloom than upwelling by ET. Aerosol precipitation in the southwestern AS also played an important role in high Chl-*a* in the deep offshore AS (i.e., Section B in Fig. 1(a)), as second only to ET and sea surface temperature (SST), and even higher than EPV. A novel finding is that the influence of aerosol optical thickness (AOT) is evident in the offshore region and the dust precipitation is more important sources to oligotrophic water. Both the stability of the upper ocean and the aerosol precipitation may play more evident roles in the open regions of the southwestern AS off Somali.

Keywords Somali Peninsula, the southwest Arabian Sea, chlorophyll-a, wind speeds, upwelling, nutrients

1 Introduction

Phytoplankton photosynthesizes in the ocean by absorbing carbon dioxide and emitting oxygen, which affects sink-emission processes of carbon dioxide. The phytoplankton growth in the ocean is largely influenced by different biogeochemical processes (Zhao and Zhang, 2014), which are generally regulated by oceanic dynamic processes. Nutrients and light are generally two key growth-limiting factors, and therefore phytoplankton growth is mainly influenced by the above factors. In the tropical/subtropical zones, light is generally rich and nutrients are generally poor in the upper 200-m ocean (Brock et al., 1991; Liu et al., 2002). The availability of nutrients in the upper ocean is mainly influenced by river discharges, atmospheric deposition, upwelling processes derived from offshore Ekman transport (ET) and wind stress curls, mixed-layer dynamics, and so on. Of these, atmospheric deposition may also be an important source of nutrients in most of the open offshore oceanic regions (Duce and Tindale, 1991; Tindale and Pease, 1999; Erickson et al., 2003; Fan et al., 2006; Kayetha et al., 2007).

Received March 1, 2021; accepted May 12, 2021

E-mail: huizhao1978@163.com

*These authors contributed equally to this work.

The Arabian Sea (AS), situated in the northern tropics, is a unique region mostly influenced by the reverse monsoons as well as dust storms, inducing high productivity in the region (Madhupratap et al., 1996; Tang et al., 2002). Smith and Codispoti (1980) observed two areas of upwelling off Somalia, one near 10°N and one near 5°N with surface Chl-*a* about 0.4–5.0 mg·m^{-3}. In addition, during the southwest monsoon, coastal upwelling occurs at 11°N in the Somali Current, where the maximum biomass value recorded is 38.0 g·m^{-2} (Couwelaar, 1997). Shafeeque et al. (2017) showed that dust aerosols enhance Chl-*a* concentration off Somalia. Singh and Patra attributed largely chlorophyll-a (Chl-*a*) blooms in the north AS to aerosol depositions (Patra et al., 2007; Singh et al., 2008), whereas earlier studies presented that the Chl-*a* blooms in the north AS were induced by uplift of nutrients possibly due to vertical mixing and the eddy-induced pumping (Tang et al., 2002). The Chl-*a* blooms might also be associated with changes in stratification of upper layers during the periods of dust storms (Luis and Kawamura, 2002). These seasonally reverse monsoon and basin-wide circulations are prevailing in the AS. In the past 30 years, uplifted dust and its long-distance transport were quite changeable due to changes of wind stress shears, land cover and precipitation patterns. The dust may also increase nutrients concentration and phytoplankton primary production in upper oceans (Baker et al., 2003; Cropp et al., 2005; Mahowald et al., 2005; Kayetha et al., 2007; Wiggert and Murtugudde, 2007), and in turn regulate population and structures of phytoplankton, leading to ecological variations. The present study is focused on the spatial and temporal patterns of wind-derived parameters, including Ekman pumping velocity (EPV), offshore ET, geostrophic flows and dust precipitation. In this sense, possible mechanisms of Chl-*a* blooms off Somalia in the southwestern AS were examined using merged satellite Chl-*a* and other remote sensing data including wind and SST, for the period of June 1998–August 2016.

2 Materials and methods

2.1 Study area and data sampling

The southwestern AS (Fig. 1(a)) (Brandt et al., 2003) lies largely in tropical zones, roughly from 5° to 15°N, where the reversal monsoons prevail in winter and summer, respectively. Our study area is situated off Somali in the southwestern AS, where upwelling/high phytoplankton Chl-*a* concentrations are prevailing in summer. To further understand frequent re-occurrence of the summer Chl-*a* blooms and roles of background factors including winds, EPV, ET, geostrophic current and aerosol played in Chl-*a* blooms, three lines (Line A, Line B, Line C in Fig. 1(a)) are chosen where the variation of Chl-*a* is evident among one another. Based on average for the regions near Line A, B, and C (i.e., the parallelogram which was built that extended one pixel left and right from each center of the chosen Line, respectively), time series data of Chl-*a*, as well as other parameters for summers were produced from 1999 to 2016, and then potential relations are investigated among them.

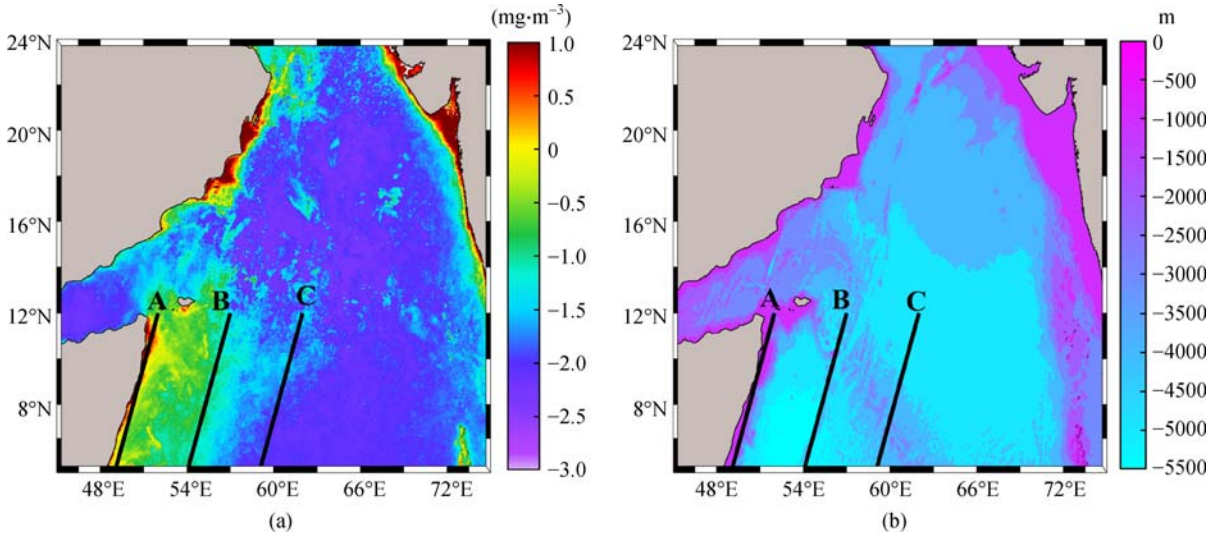

Fig. 1 (a) The spatial distribution of Chl-*a* in June of 1998–2016. The Chl-*a* is processed by logarithm with base of 10. (b) Depth map of the Arabian Sea. Line A, coastal line; Line B, the edge of upwelling; Line C, the non-upwelling area. (The shoreline and bathymetry data in Fig. 1 are obtained from Global Self-consistent, Hierarchical, High-resolution Geography Database (GSHHG) (Wessel and Smith, 1996) and 2 arc-minute Gridded Global Relief Data (ETOPO2v2) (National Geophysical Data Center, 2006), respectively. This work is licensed under a Creative Commons Attribution 4.0 International License (National Geophysical Data Center/NESDIS/NOAA/U.S. Department of Commerce, 2001)).

2.2 Satellite products

The monthly merged L3 ocean color products were generated by the GlobColor project and derived from 4 different sensors of Sea WiFS, MODIS, MERIS and VIIRS, using the (Garver-Siegel-Maritorena) GSM model (Maritorena and Siegel, 2005). The normalized reflectance data at the different wavelengths were processed by the GSM method. The monthly Chl-*a* and aerosol optical thickness of T865 (AOT) at 4 km spatial resolution were used for the period of June 1998–August 2016 in the present study. The influence of dust indexed by AOT was investigated through analysis of the relation between the aerosol depth (i.e., AOT) and the Chl-*a* concentration in the southwestern AS.

The Sea Surface Temperature (SST) and Sea Surface Wind (SSW) data at 0.125° spatial resolution are obtained from the European Centre for Medium-Range Weather Forecasts. The monthly products are used from January 1998 to December 2016. Moreover, Chl-*a*, AOT, SST, SSW, and SSW-derived EPV and ET in the region are investigated to clarify change of phytoplankton Chl-*a*, and possible roles of the aerosol and wind fields played in the western AS.

Geostrophic velocity data at 0.25° spatial resolution during January 1998 to December 2016 were obtained from AVISO (the Archiving, Validation and Interpretation of Satellite Oceanographic data set). The monthly products of geostrophic velocities were only utilized for the same period in the upwelling processing.

2.3 Data processing and methods

2.3.1 Chl-*a*, AOT, and SST

In consideration of few valid pixels in the daily Chl-*a* products due to bad weather conditions in the western Arabian Sea, the monthly Chl-*a* products are used in the study. The monthly Chl-*a* climatologies (i.e., June, July, and August) during summer are first presented for each year. Afterwards, the monthly products of Chl-*a*, AOT, and SST were further sampled along Line B during 1998–2016 and were processed into the time series. Based on analysis of the inter-annual change of Chl-*a*, AOT, and SST, responses of the Chl-*a* blooms to oceanic conditions will be probed.

2.3.2 Upwelling intensity

Offshore transport triggered by winds parallel to the coastlines, EPV, and onshore geostrophic flows can regulate upwelling intensity in the coastal regions. In this study, ET, EPV, and geostrophic transport (T_G) was used to evaluate the possible vertical transport induced by the wind fields and the geostrophic flow in the chosen region (Line A and B in Fig. 1(a)), where strong winds and geostrophic flows prevail in summer.

Wind-triggered vertical movement is mainly derived from the following two ways: Ekman offshore transport induced by the wind stress components parallel to the coastline, and EPV triggered by the wind stress curls. Since coastal upwelling intensity is partially regulated by the geostrophic current (Marchesiello and Estrade, 2010), its effect of geostrophic current should be considered. Based on the method of Messie and Chavez (Messié and Chavez, 2015), the coastal upwelling transport (ET, $m^2 \cdot s^{-2}$) and other factors can be expressed as

$$\mathrm{ET} = T_{\mathrm{Ek}} + T_{\mathrm{G}}, \tag{1}$$

$$T_{\mathrm{Ek}} = -\frac{\tau_{\mathrm{alongshore}}}{\rho_w f}, \tag{2}$$

$$\tau_{\mathrm{alongshore}} = \rho_{\mathrm{air}}\ C_{\mathrm{D}} U^2, \tag{3}$$

$$C_{\mathrm{D}} = 10^{-3}(0.60 + 0.071U)\left(6 \leqslant U \leqslant \frac{26\ m}{s}\right), \tag{4}$$

$$\mathrm{EPV} = \frac{\mathrm{curl}(\tau)}{\rho f} + \frac{\beta \tau_x}{\rho f^2}, \tag{5}$$

$$T_{\mathrm{G}} = -U_{\mathrm{G}} D_{\mathrm{Ek}} \ \text{if}\ \ U_G < 0,$$

$$T_{\mathrm{G}} = -0.5(U_{\mathrm{G}} D_{\mathrm{Ek}}) \ \text{if}\ \ U_{\mathrm{G}} \geqslant 0, \tag{6}$$

where T_{Ek} is the Ekman transport ($m^2 \cdot s^{-1}$), EPV is the Ekman pumping velocity ($m \cdot s^{-1}$) induced by wind stress curls, and T_{G} is the transport ($m^2 \cdot s^{-1}$) induced by geostrophic currents. The calculation method of geostrophic transport was described by Marchesiello and Estrade (2010). Ekman transport is the coastal upwelling occurring within a distance of 100 km from the coastline (i.e., within the first Rossby deformation radius (R_0 = ~100 km in the study area with a mean latitude of about 10ºN (Chelton et al., 1998)). The $\tau_{\mathrm{alongshore}}$ is components of the wind stress parallel to the coastline positive northeastward, and f is Coriolis parameter (s^{-1}); ρ_{w} and ρ_{air} are the densities of seawater ($kg \cdot m^{-3}$) and air, respectively; C_{D} is wind drag coefficient, U is the wind speed; U_{G} is the offshore or onshore geostrophic current, and D_{Ek}, the Ekman depth was calculated with the equation $D_{\mathrm{Ek}} = 3.8U/\sqrt{\sin\phi}$, where the constant of 3.8 is based on ρ_{w} = 1025 $kg \cdot m^{-3}$, ρ_{air} = 1.25 $kg \cdot m^{-3}$, and the drag coefficient in the study area $C_{\mathrm{D}} = 1.32 \times 10^{-3}$ for the typical Ekman's value (Vickers et al., 2013); τ_x is the latitudinal wind stress components (Pa), curl (τ) is the wind stress curl ($Pa \cdot m^{-1}$), and β is the meridional derivative ($m^{-1} \cdot s^{-1}$) of f. The nutrients in the surface are probably exhausted before the surface water masses sinking again, and thus negative EPV (Messié et al., 2009) is set to 0 when averaging for the study area.

2.3.3 Time series of Chl-*a*, AOT, SST, T_{Ek} and EPV

High Chl-*a*, strong wind and high AOT in summer prevail in the southwestern AS. Due to lack of valid pixels under influence of clouds in remote sensing ocean color (Fig. 2), in the study we mainly considered the region off the Somali coast (Line A and B in Fig. 1(a)) where more valid data was available and there were higher Chl-*a* concentrations. In addition, it is important to take into account that satellite data of Chl-*a* near coast could present overestimations due to the presence of other material in the ocean surface (for example, sediment resuspension). In our study region, the Chl-*a* concentration (~0.6–2.5 mg·m^{-3}) in the vicinity of line A is consistent with Smith and Codispoti (1980) (~0.4–3.0 mg·m^{-3}) and Couwelaar (1997) (~0.4–2.5 mg·m^{-3}). Therefore, we believe that the remote sensing observations off the Somali coast are available. To investigate quantitative roles of ocean conditions played in high summer Chl-*a* concentrations in the region, the time series data of Chl-*a*, AOT, SST, T_{Ek}, EPV, and T_G are produced through averaging parameters spatially (Line A and B in Fig. 1(a)). Then, we also use the multiple and partial correlations to document the roles of SST, dust precipitation indexed by AOT, wind-induced ET, wind-induced EPV, and SST in the strength of summer blooms over the western AS. The multiple correlation analysis (Liu et al., 2002) is a statistical method that predicts values of one variable in terms of two or more other variables. Given the simple correlation coefficient matrix among the variables of x_1, x_2, … , x_m, and y, the multiple correlation the coefficient and partial correlation coefficients can be computed as follows:

$$R = \begin{bmatrix} r_{11} & r_{12} & & r_{1m} & r_{1y} \\ r_{21} & r_{22} & & r_{2m} & r_{2y} \\ \vdots & \vdots & \vdots & \vdots & \vdots \\ r_{m1} & r_{m2} & & r_{mm} & r_{my} \\ r_{y1} & r_{y2} & & r_{ym} & r_{yy} \end{bmatrix}. \quad (7)$$

The definition of multiple correlation coefficients is as follows:

$$R_{y\cdot 1,2,\ldots,m} = 1 - \sqrt{\frac{|R|}{R_{yy}}}, \quad (8)$$

and partial correlation coefficients between x_i and y is calculated by

$$R_{yi\cdot 1,2,\ldots,m} = \frac{R_{yi}}{\sqrt{R_{yy}R_{ii}}}, \quad (9)$$

where y is the dependent and x_1, x_2, …, x_m is the causative variable; the multiple correlation coefficient, $|R|$ is the determinant of the matrix R; R_{yy}, R_{ii}, and R_{yi} are the algebraic complements of r_{yy}, r_{ii}, and r_{yi} in the correlation coefficient matrix R, respectively. Here r_{ij} is the simple correlation coefficient between x_1, x_2, … , x_m, and y.

2.3.4 Empirical Orthogonal Function (EOF)

The EOF (Empirical Orthogonal Function), also known as principal component analysis and eigenvector analysis, is a mathematical method for extracting data eigenvectors and analyzing the matrix structure.

The EOF analysis steps are as follows:

1) Perform anomaly processing on the initial data to get matrix $(A_{i\times j})$.

2) Calculate the cross multiplication of A and its transposed A^T to obtain a square covariance matrix $\left(B_{i\times j} = \frac{1}{n}A \times A^T\right)$.

3) Calculate the characteristic root vector $(C_{i\times j})$ and eigenvector $(D_{i\times j})$, both of which satisfy the following relationship:

$$B_{i\times j} \times D_{i\times j} = D_{i\times j} \times C_{i\times j}. \quad (10)$$

The characteristic root corresponds to the eigenvector, which is called the spatial mode.

4) Project the spatial modal to the original data A, and then the principal components corresponding to the spatial modal can be obtained:

$$PC_{i\times j} = D^T_{i\times j} \times A_{i\times j}. \quad (11)$$

The row vector of the principal component is the time coefficient corresponding to the spatial mode.

3 Results

3.1 Summer high Chl-*a* concentrations in the southwestern AS

In summer, the monthly Chl-*a* climatologies (Fig. 2) presented generally high Chl-*a* concentrations in the western AS. Compared with that in Jun, higher Chl-*a* (>0.6 mg·m^{-3}) during July–August was observed in the AS, especially in the region off Somalia in western AS. Fig. 3 shows the general seasonal cycle and inter-annual variation of Chl-*a* distribution in the western AS (Section A and Section B) during the period 1998–2016. High Chl-*a* in Section A, especially in June 2005 (>8 mg·m^{-3}), June 2011 (>9 mg·m^{-3}) and June 2016 (>8 mg·m^{-3}). Chl-*a* data in the north AS (Fig. 2) are largely unavailable due to the influence of heavy cloud or heavy dust aerosol in the sky on the ocean color sensor. Therefore, we focused mainly on the high Chl-*a* patch and ocean conditions offshore of the Somali coastlines in the western AS, where there is also better data coverage in ocean color observations.

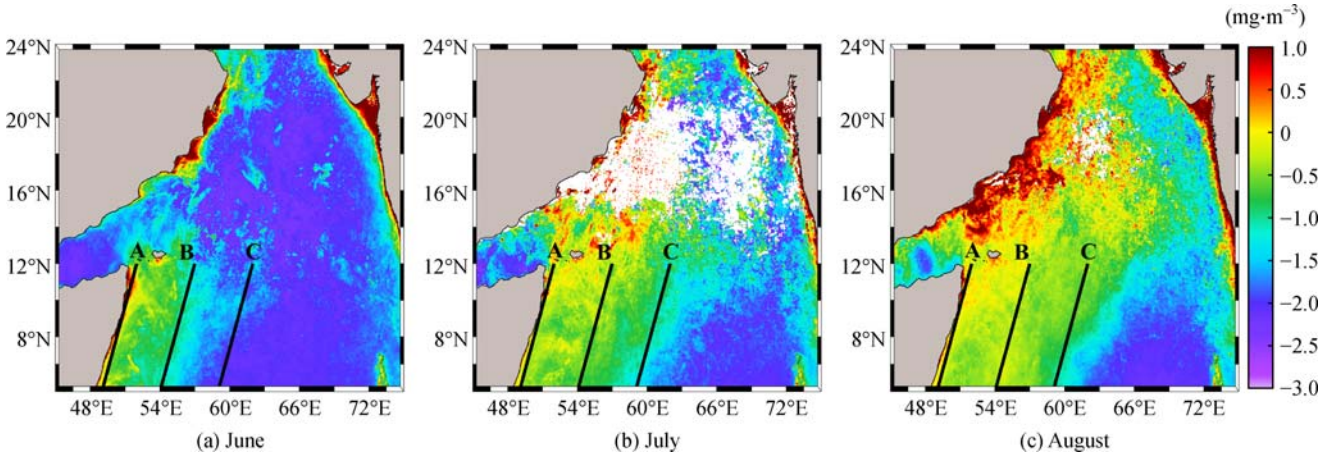

Fig. 2 Monthly climatology of chlorophyll a in (a) June, (b) July and (c) August averaged for the period of 1998–2016. The Chl-*a* is processed by logarithm with base of 10. (The shoreline and bathymetry data in Fig. 2 are obtained from Global Self-consistent, Hierarchical, High-resolution Geography Database (GSHHG) (Wessel and Smith, 1996) and 2 arc-minute Gridded Global Relief Data (ETOPO2v2) (National Geophysical Data Center, 2006), respectively. This work is licensed under a Creative Commons Attribution 4.0 International License (National Geophysical Data Center/NESDIS/NOAA/U.S. Department of Commerce, 2001).)

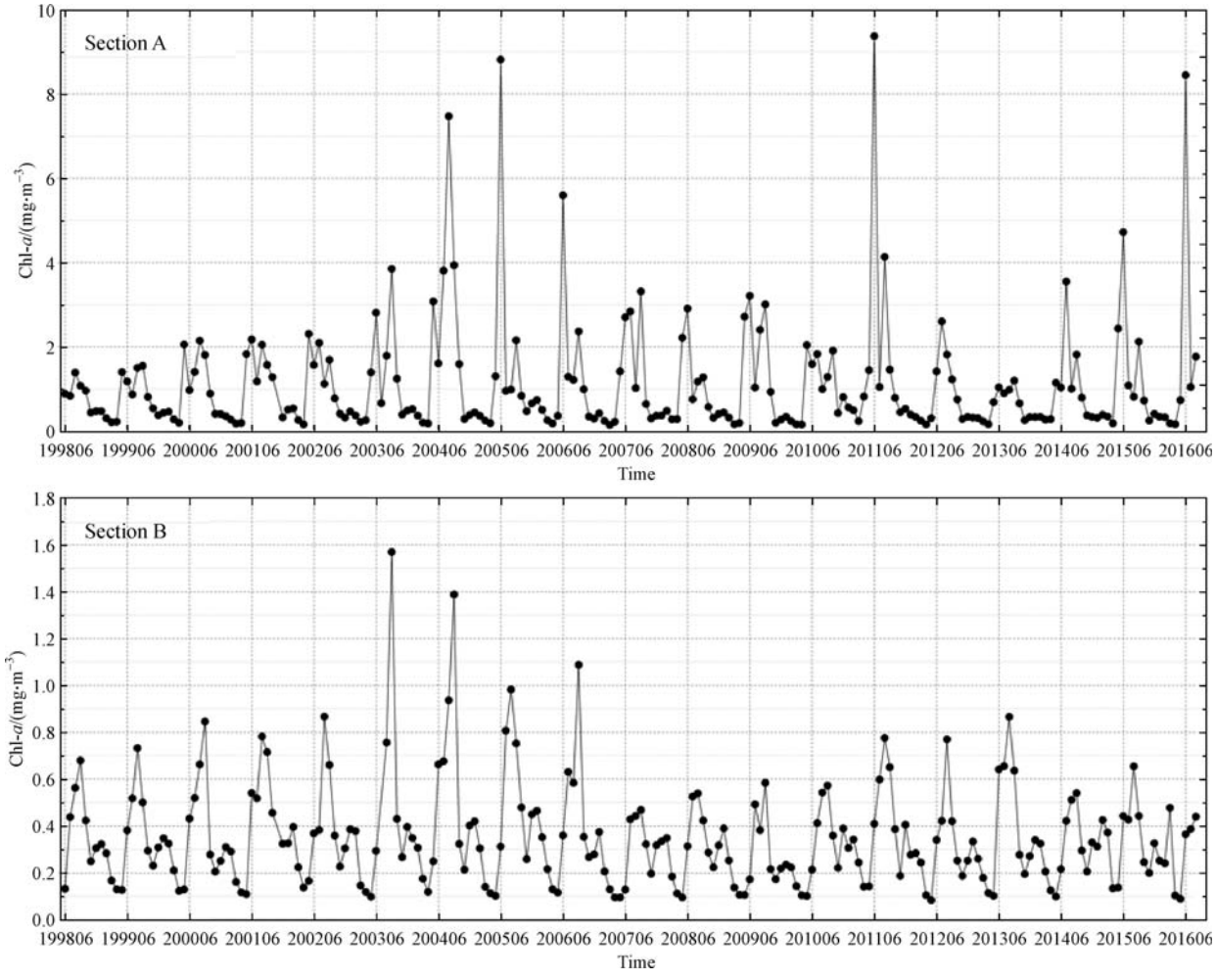

Fig. 3 Time-series of the summer Chl-*a* concentration in Section A and Section B from 1998 to 2016.

3.2 Distribution of SST, EPV and AOT in summer

There were high SSTs (~30°C) in the eastern AS and low SSTs (~25°C; Fig. 4(a)) in the western AS, especially in the coastal regions north-east of the Somali Peninsula and east of the Arabian Peninsula. South-westerly winds (Fig. 4(b)) prevail in the months of summer, with stronger wind (>12 m·s^{-1}) in the western AS. The climatology of wind-derived EPV (Fig. 4(c)) indicated strong upwelling tendency (~2.5×10^{-5} m·s^{-1}) off the Peninsula in the southwestern AS, and weak upwelling or downwelling (~ -1×10^{-5} m·s^{-1}) offshore of the Arabian Peninsula in the north-western AS. The AOT (Fig. 4(d)) presented high concentrations in the northern AS and low concentrations in the southern AS, which suggests that possible dust precipitations were more popular in the northern than the southern AS, roughly coinciding with the pattern of the Chl-*a* climatology (Fig. 2).

3.3 EOF analysis of Chl-*a* and oceanic conditions

The results of the first EOF modes for summer months (i.e., 3 months of June–August) from 1998 to 2016 were presented in Fig. 5 to show spatial and temporal variations of Chl-*a* concentrations along with SST and AOT in the offshore region off Peninsula. The first principal components (PCs) of Chl-*a*, SST, and AOT (Fig. 5) displayed significant annual and intra-seasonal variations. The first EOF mode of Chl-*a* explains 29.5% of the variance, suggesting the factors also regulating possibly Chl-*a* concentration in the region. Compared with that of Chl-*a*, the first mode of SST explains 82.8% of the variance, and the first mode of AOT accounted for 16.2% of the variances. The variance of SST was evident between north and south of the study area, with a tendency of strong (weak) variation in the central-east (the offshore-central region) of the study area. The spatial pattern of AOT displayed higher (lower) variations in the coastal (offshore) region. The higher AOT variance (Fig. 5(c)) appeared near Line A in coastal regions with low variance near Lines B and C in the offshore region.

3.4 Correlation analysis between Chl-*a* and oceanic conditions

The scattergraphs (Fig. 6) of Chl-*a* vs SST, wind EPV, ET, and AOT respectively, presented a good coherent tendency with proportional variation each other. The simple correlation analysis (Table 1) indicated significant correlation between Chl-*a* vs SST, ET, EPV and AOT. The Chl-*a* was positively correlated with EPV, ET, and AOT, and had a strong negative correlation with SST. The above correlations suggested that Chl-*a* concentration may be regulated mainly by vertical transport induced by ET and EPV, dust precipitation indexed by AOT and stability of upper water indexed by SST.

3.5 Time series of Chl-*a* and environmental conditions

To analyze further the roles played by SST, wind ET, EPV, and AOT in the increase of Chl-*a* concentrations, the multiple correlation/partial analyses were employed in the study. The stronger correlation was presented between Chl-*a* concentration (as the dependent variable) and oceanic conditions (as the causative variables), indicating the above factors can explain the increase of Chl-*a* to a great extent. Though the above factors may exert important impacts on the phytoplankton Chl-*a* increase, the influence of each factor was different according to the results of the partial correlation analysis (Table 2). In the following partial correlation analysis, environmental variables with the lowest correlation coefficient are removed in turn and only a few significant variables are left at last. In Section A, wind speed with the least correlation coefficients of 0.01 with Chl-*a* was thereby removed when we further estimated the importance of each causative variable. After wind speed removed, the coefficient of AOT with Chl-*a* became the smallest, so, we next removed AOT. Finally, there exist only three variables (EPV, SST, and ET) with the highest correlation with Chl-*a*. In the above causative variables, the coefficients of Chl-*a* with SST, EPV, and ET are more significant, suggesting that upwelling triggered by EPV, instability inferred by SST and the offshore ET exerted more important impacts on Chl-*a* increase near the coast. The direct contributions of wind and dust precipitation were relatively weak, compared with those of SST, ET, and EPV. In contrast, SST and AOT appear to play more important roles in the Chl-*a* increase in the upwelling area along Section B.

4 Discussion

4.1 The summer phytoplankton blooms off the Somali coast

In tropical oceans with abundant illumination, available nutrients are generally a limiting factor in the euphotic layer, due to consumption and absorption of phytoplankton and barrier of nutrients injection into the upper layer by existence of thermocline in the upper oceans. Water temperature decreases gradually with depth below the upper mixed layer. During the summer period the south-westerly wind systems favor strong upwelling, biological productivity is higher, particularly off the Somali coast in the South-western Arabian Sea (Madhupratap et al., 1996; Prasanna Kumar et al., 2002). Upwelling as an important role in the redistribution of marine nutrients can entrain nutrients from deeper layers closer to the surface, fueling phytoplankton blooms.

In our study region, high Chl-*a* concentration and upwelling were verified according to the horizontal distribution of summer climatology of Chl-*a* and SST (Fig. 2, Fig. 4(a)), consistent with Brock et al. (1991) and

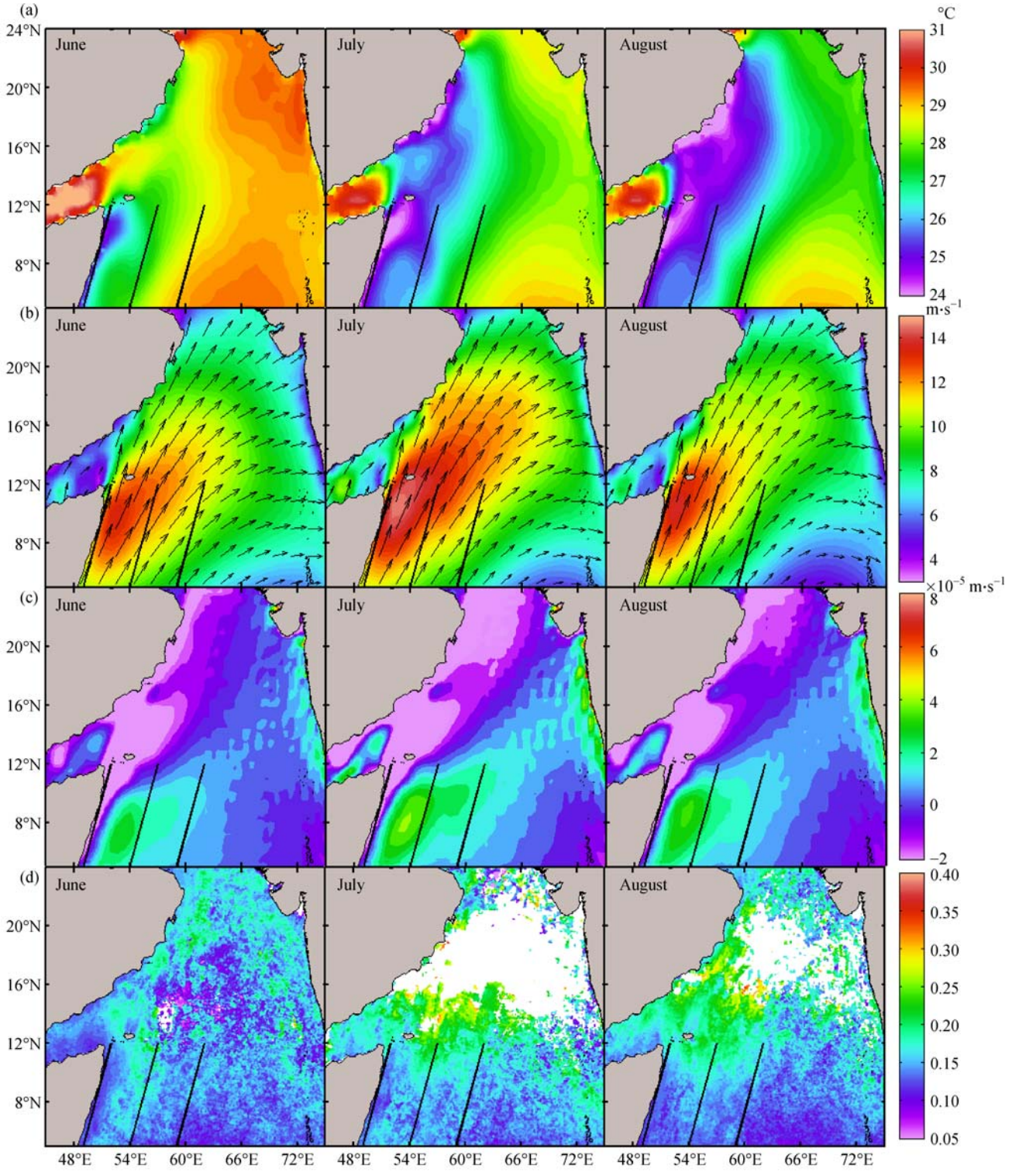

Fig. 4 Summer climatologies of (a) SST, (b) wind speed, (c) EPV and (d) AOT averaged for the period of 1998–2016. (The shoreline and bathymetry data in Fig. 4 are obtained from Global Self-consistent, Hierarchical, High-resolution Geography Database (GSHHG) (Wessel and Smith, 1996) and 2 arc-minute Gridded Global Relief Data (ETOPO2v2) (National Geophysical Data Center, 2006), respectively. This work is licensed under a Creative Commons Attribution 4.0 International License (National Geophysical Data Center/NESDIS/NOAA/U.S. Department of Commerce, 2001).)

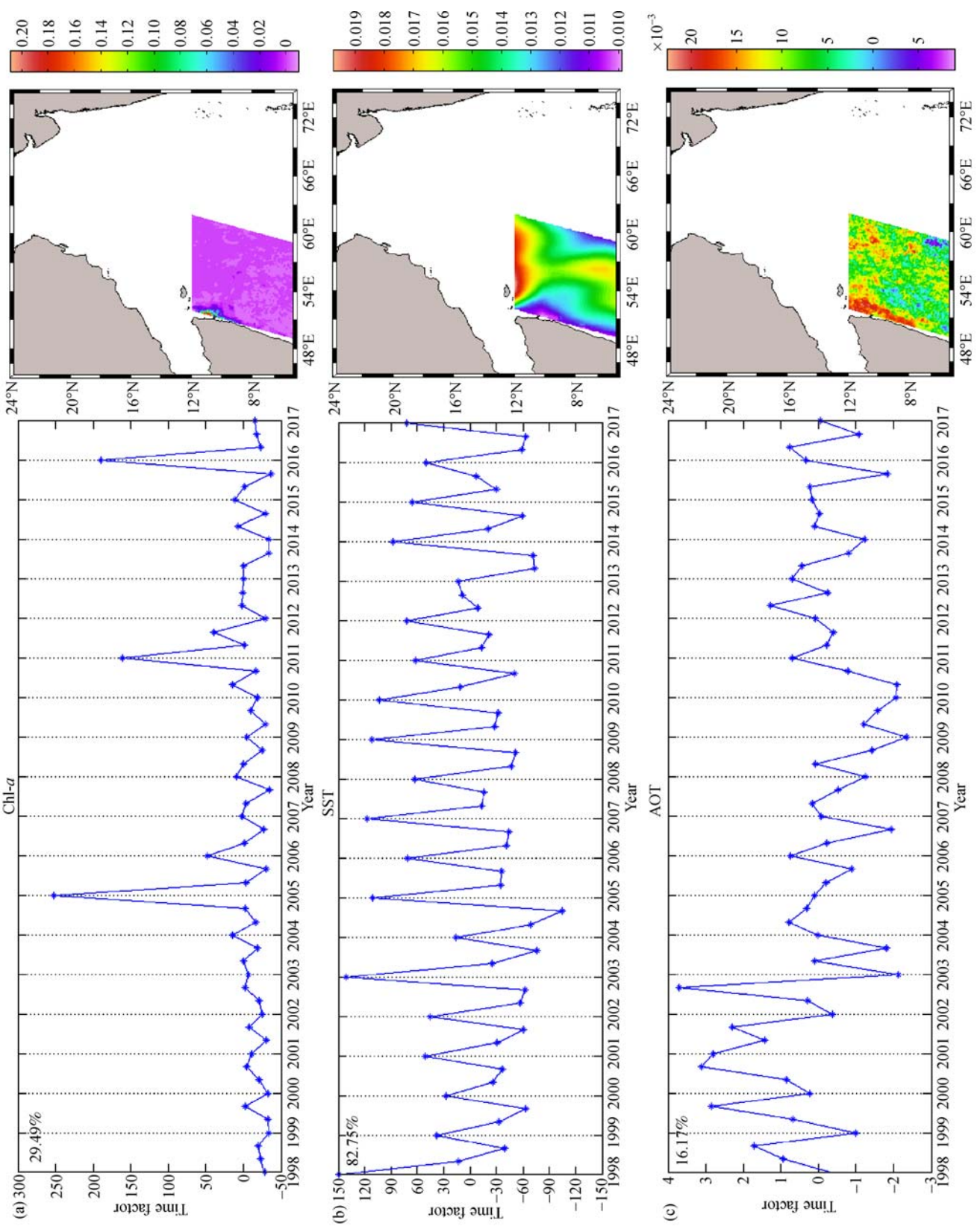

Fig. 5 The leading EOF modes of (a) Chl-*a*, (b) SST, and (c) AOT. The left panel is the first PC; the right is the spatial mode.

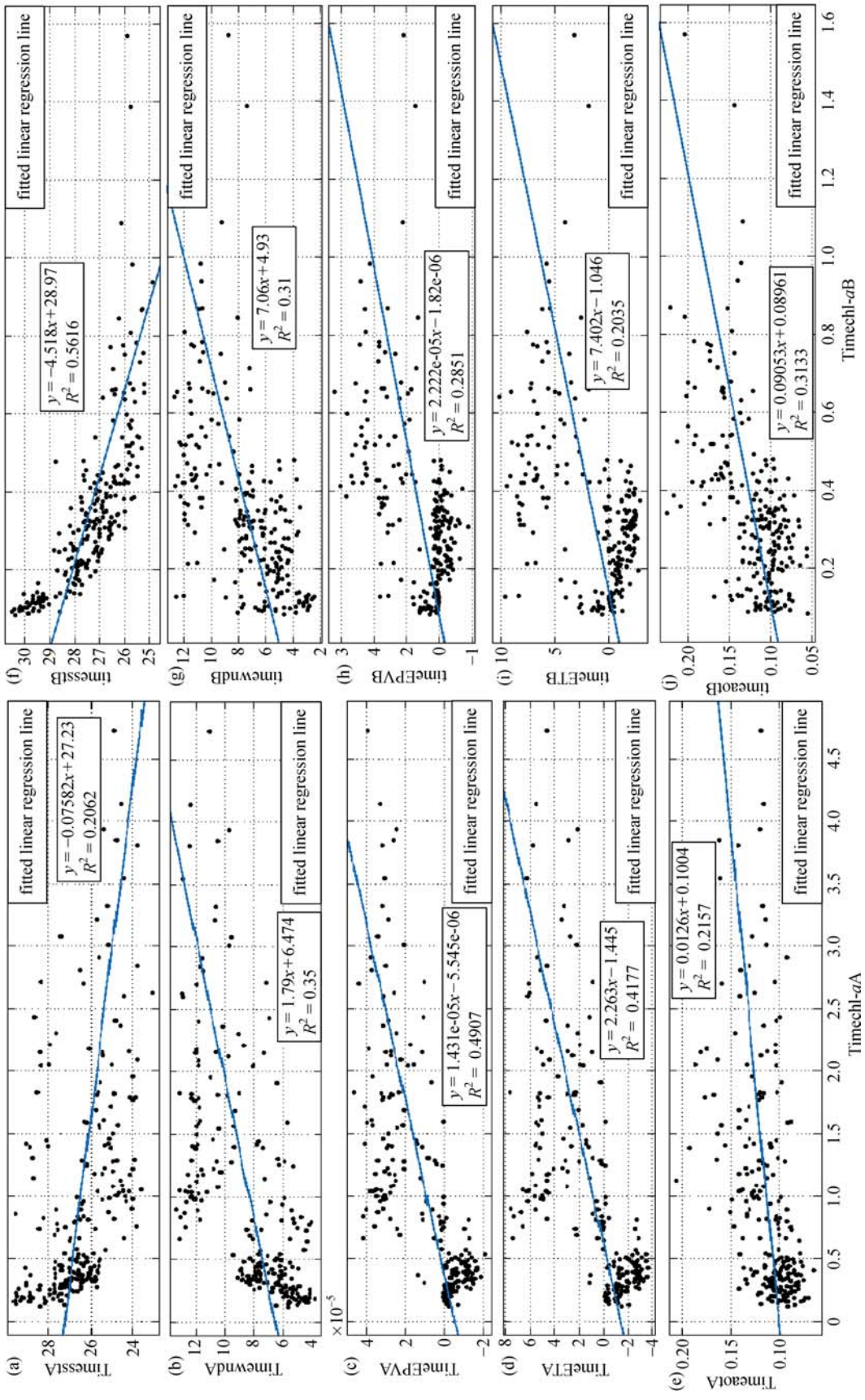

Fig. 6 Scattergraphs of Chl-*a* vs. (a) SST, (b) wind, (c) EPV, (d) ET, (e) AOT averaged along Section A and (f) SST, (g) wind, (h) EPV, (i) ET, (j) AOT averaged along Section B with the correlation coefficients.

Table 1 The simple correlation between Chl-*a* concentration and other oceanic conditions along sections A and B. Data used in the simple correlation analysis is derived from average of Chl-*a* and other parameters along the sections

Chl-*a*	Simple correlation coefficients				
	SST	Wind	EPV	ET	AOT
Section A	−0.45	0.59	0.70	0.65	0.46
Section B	−0.75	0.56	0.53	0.45	0.56

Broerse et al. (2000). In summer, strong south-westerly wind is prevailing over the western AS, shaping a low-level jet named with the Findlater Jet (Findlater, 1969). As presented in the pattern of SST (Fig. 4(a)), the jet may lead to strong surface cooling/low SST related to the increase in latent and sensible heat loss, intensifying vertical mixing and upwelling of subsurface layer water with high nutrients. The component of this wind jet parallel to the coastline induces the formation of strong coastal upwellings in the coastal regions of Somalia. Lateral changes in wind stresses north of the wind jet induce also EPV, triggering upwelling in the open western AS (Lee et al., 2000). The above strong upwellings result in upward transport of cooler, nutrient-rich water from subsurface into surface. Merged with the influence of the horizontal flow, evident phytoplankton Chl-*a* blooms appear frequently and high phytoplankton biomass extends offshore from the coasts of Oman and Somalia almost to the central AS. Compared with line B and line C, higher Chl-*a* (> 2.0 $mg \cdot m^{-3}$) during summer was observed on line A (Fig. 2). Coinciding roughly with the line A of high Chl-*a*, lower SST and stronger wind speed were displayed respectively in the same region (Figs. 4(b) and 4(c)). Moreover, the EOF1 of Chl-*a* (Fig. 5(a), right panel) shows the distribution characteristics of high Chl-*a* concentration near line A of the study area, while the EOF1 of SST (Fig. 5(b), right panel) has a low-value area on line A corresponds to the high Chl-*a* value of the A-line. Fig. 5(a), left panel shows an anomaly high values of time factor at Jun 2005, Jun 2011 and Jun 2016. It is showed that the Chl-*a* is abnormally high in these three years, which is consistent with section A of Fig. 3. Lower SST, atmospheric deposition and terrestrial inputs may be responsible for higher phytoplankton on line A than that in summer. In addition, the dust deposition in air is also an important iron source in the open or coastal sea (Duce and Tindale, 1991). Patra et al. (2007) thought the aerosol mineral deposition was one important nutrient source, triggering the phytoplankton blooms in winter in the northern AS. Singh et al. (2008) affirmed also dust deposition exerted an important influence on the Chl-*a* increase of the northern AS. Consistent with the previous studies, our results from the EOF1 (Fig. 5(a), right panel) of AOT showed the high value mainly distributed near the A line. It is indicated that atmospheric deposition can directly transport nutrients such as nitrogen, phosphorus, potassium, etc. to the ocean through rainfall, evaporation, which directly act on the ocean and cause phytoplankton blooms.

4.2 Possible environmental factors regulating the summer phytoplankton blooms

Our study area, belongs to tropical sea, is of adequate light in upper layers (Liu et al., 2002) and high sea surface temperature in the study area in summer (Section A, B in Fig. 4(a)). Therefore, our study focused mainly on responses of summer phytoplankton blooms to physical processes that influence nutrient supply. The influence of dust precipitation, the transport of ocean currents, the upwelling induced by wind stress curls and offshore ET, and SST were investigated to identify possible mechanism of blooms in the region. The results from the simple correlation analysis (Table 1) indicated all upwelling by ET and EPV, mixing indexed by SST, along with the dust precipitation indexed by AOT exerted apparent influences on the dynamics of nutrients and then phytoplankton blooms in our study region. However, contribution of each factor can be different to the Chl-*a* bloom. The stepwise regression analysis displayed the better correlations existed between Chl-*a* with EPV ($r = 0.42$), ET ($r = 0.26$), and SST ($r = 0.22$). It is showed that the instability of upper oceans caused by the upwelling triggered by offshore ET and EPV in the study area (Section A in Table 2) is higher than the direct influence of wind and AOT. ET during summer can force the seaward transport of surface coastal waters and carry nutrient-rich deeper water into the coastal surface layer in the amount that compensates the horizontal mass loss in the coastal region. Positive EPV, resulting from wind stress curls, can induce uplift of deeper water from subsurface (Liao et al., 2016; Zhao and Wang, 2018; Zhao et al., 2018). Since the seawater temperature decreases usually with depth below the mixed layer, the uplifted water is generally colder than the surface water displaced by it. Moreover, the upwelled water has often higher nutrients concentrations than the old surface water, for nutrients in the surface water have been largely depleted by the growth of phytoplankton. The results from the stepwise regression analysis suggested further that EPV-induced upwelling may be more helpful than the ET-induced upwelling in the coastal region off Somalia, leading to probably more significant influence of EPV upwelling (i.e., wind stress curls) on the phytoplankton bloom than upwelling by ET, roughly coincided with previous studies (Lee et al., 2000; Wiggert et al., 2005, 2006). Moreover, it was easy to receive terrestrial sources with rich nutrients in the coastal region (i.e., Line A in Fig. 1(b), compared with that in the offshore region (near Line B in Fig. 1(b)).

Table 2 The multiple correlation coefficients and partial correlation coefficients among Chl-*a* and other oceanic factors

Section A	SST	Wind	EPV	ET	AOT	Multiple correlation
Chl-*a*	−0.14	0.01	0.42	0.27	0.08	0.74
Chl-*a*	−0.20		0.43	0.27	0.09	0.74
Chl-*a*	−0.22		0.42	0.26		0.73
Section B	SST	Wind	EPV	ET	AOT	Multiple correlation
Chl-*a*	−0.64	−0.23	−0.04	0.18	0.24	0.80
Chl-*a*	−0.66	−0.24		0.24	0.23	0.80
Chl-*a*	−0.67			0.12	0.18	0.79
Chl-*a*	−0.67				0.36	0.79

Therefore, the AOT may exert more important impact on Chl-*a* only in the offshore region, implied by Section B in Table 2. The closer correlation coefficient between Chl-*a* and SST in the offshore region may be attributed to the facts that SST not only is a good proxy of the upwelling intensity (Zhao and Tang, 2007; Benazzouz et al., 2014), but also an index of instability of the upper ocean, because lower SST would enhance instability of the upper ocean, favorable to vertical mixing and vertical exchange, increasing nutrients in the eutrophic layer. Therefore, variation of SST can reflect better effect of upwelling (Table 2) and instability of upper oceans, resulting in the better correlation observed between Chl-*a* and SST. This may also lead to the phenomena that good correlation between SST and Chl-*a* concentration in the partial correlation analysis wherever in the coastal or the offshore region. Hence, we conjectured that the phytoplankton blooms observed Somali coast may be mainly triggered by increasing nutrient level through the upwelling triggered by EPV (and ET) and strong entrainment mixing associated with strong wind and heat loss. A novel finding is that the influence of AOT in the study area is evident in the offshore region, and the dust precipitation is more important sources to oligotrophic water. Both the stability of upper ocean and the aerosol precipitation may play more evident roles in open regions of the southwestern AS off Somali.

5 Conclusions

The distinct high Chl-*a* concentrations were observed in the southwestern AS, especially off the Somali coast. The summer Chl-*a* off the Somali coast presented strong inter-annual variations, along with wind-induced ET and EPV in the southwestern AS. In the center of the upwelling, Chl-*a* was well correlated with ET, EPV and SST, which implied that offshore transport, upwelling and sea surface cooling played probably important roles in the phytoplankton bloom, by supply of nutrients from coastal regions to offshore regions and from the subsurface to the upper layer through favorable vertical mixing and vertical exchange. AOT appears to play more important role in the algal blooms in the offshore than the coastal regions off Somalia.

Acknowledgements The present research is supported by the National Natural Science Foundation of China (Grant No. 42076162), the Natural Science Foundation of Guangdong Province, China (No. 2020A1515010496) and project supported by Innovation Group Project of Southern Marine Science and Engineering Guangdong Laboratory (Zhuhai) (No. 311020004). We thank GlobColor's Working Group for providing merged Chl-*a* data (available at ACRI website) and the European Centre for Medium-Range Weather Forecasts for providing monthly SST and SSW products (available at ECMWF webstie).

References

Baker A R, Kelly S D, Biswas K F, Witt M, Jickells T D (2003). Atmospheric deposition of nutrients to the Atlantic Ocean. Geophys Res Lett, 30(24): 2296

Benazzouz A, Mordane S, Orbi A, Chagdali M, Hilmi K, Atillah A, Lluís Pelegrí J, Hervé D (2014). An improved coastal upwelling index from sea surface temperature using satellite-based approach-The case of the Canary Current upwelling system. Cont Shelf Res, 81: 38–54

Brandt P, Dengler M, Rubino A, Quadfasel D, Schott F (2003). Intraseasonal variability in the southwestern Arabian Sea and its relation to the seasonal circulation. Deep Sea Res Part II Top Stud Oceanogr, 50(12–13): 2129–2141

Brock J C, McClain C R, Luther M E, Hay W W (1991). The phytoplankton bloom in the northwestern Arabian Sea during the southwest monsoon of 1979. J Geophys Res, 96(C11): 20623–20642

Broerse A T C, Brummer G J A, Van Hinte J E (2000). Coccolithophore export production in response to monsoonal upwelling off Somalia (northwestern Indian Ocean). Deep Sea Res Part II Top Stud Oceanogr, 47(9–11): 2179–2205

Chelton D B, deSzoeke R A, Schlax M G, El Naggar K, Siwertz N (1998). Geographical variability of the first baroclinic Rossby radius of deformation. Phys Oceanogr, 28(3): 433–460

van Couwelaar M(1997). Zooplankton and micronekton biomass off Somalia and in the southern Red Sea during the SW monsoon of 1992 and the NE monsoon of 1993. Deep Sea Res Part II Top Stud Oceanogr, 44(6–7): 1213–1234

Cropp R A, Gabric A J, Mctainsh G H, Braddock R D, Tindale N (2005). Coupling between ocean biota and atmospheric aerosols: dust,

dimethylsulphide or artifact? Global Biogeochem Cycles, 19(4): GB4002

Duce R A, Tindale N W (1991). Atmospheric transport of iron and its deposition in the ocean. Limnol Oceanogr, 36(8): 1715–1726

Erickson D J III, Hernandez J L, Ginoux P, Gregg W W, McClain C, Christian J (2003). Atmospheric iron delivery and surface ocean biological activity in the Southern Ocean and Patagonian region. Geophys Res Lett, 30(12): 1609

Fan S M, Moxim W J, Levy H I I II (2006). Aeolian input of bioavailable iron to the ocean. Geophys Res Lett, 33(7): L07602

Findlater J (1969). A major low-level air current near the Indian Ocean during the northern summer. Q J R Meteorol Soc, 95(404): 362–380

Kayetha V K, Senthil Kumar J, Prasad A K, Cervone G, Singh R P (2007). Effect of dust storm on ocean color and snow parameters. J Indian Soc Remote Sens, 35(1): 1–9

Lee C M, Jones B H, Brink K H, Fischer A S (2000). The upper-ocean response to monsoonal forcing in the Arabian Sea: seasonal and spatial variability. Deep Sea Res Part II Top Stud Oceanogr, 47(7–8): 1177–1226

Liao X, ZhanH, Du Y (2016). Potential new production in two upwelling regions of the western Arabian Sea: estimation and comparison. J Geophys Res Oceans, 121(7): 4487–4502

Liu K K, Chao S Y, Shaw P T, Gong G C, Chen C C, Tang T Y (2002). Monsoon-forced chlorophyll distribution and primary production in the South China Sea: observations and a numerical study. Deep Sea Res Part II Top Stud Oceanogr, 49(8): 1387–1412

Luis A J, Kawamura H (2002). Mechanism for sea surface temperature cooling in the Gulf of Oman during winter. Geophys Res Lett, 29 (11): 1521

Madhupratap M, Kumar S P, Bhattathiri P M A, Kumar M D, Raghukumar S, Nair K K C, Ramaiah N (1996). Mechanism of the biological response to winter cooling in the northeastern Arabian Sea. Nature, 384(6609): 549–552

Mahowald N M, Baker A R, Bergametti G, Brooks N, Duce R A, Jickells T D, Kubilay N, Prospero J M, Tegen I (2005). Atmospheric global dust cycle and iron inputs to the ocean. Global Biogeochem Cycles, 19(4): GB4025

Maritorena S, Siegel D A (2005). Consistent merging of satellite ocean color data sets using a bio-optical model. Remote Sens Environ, 94 (4): 429–440

Marchesiello P, Estrade P (2010). Upwelling limitation by onshore geostrophic flow. J Mar Res, 68(1): 37–62

Messié M, Chavez F P (2015). Seasonal regulation of primary production in eastern boundary upwelling systems. Prog Oceanogr, 134: 1–18

Messié M, Ledesma J, Kolber D D, Michisaki R, Foley D G, Chavez F P (2009). Potential new production estimates in four eastern boundary upwelling ecosystems. Prog Oceanogr, 83(1–4): 151–158

National Geophysical Data Center (2006). 2-minute Gridded Global Relief Data (ETOPO) v2. National Geophysical Data Center, NOAA

National Geophysical Data Center/NESDIS/NOAA/U.S. Department of Commerce (2001). ETOPO2, Global 2 Arc-minute Ocean Depth and Land Elevation from the US National Geophysical Data Center (NGDC). Research Data Archive at the National Center for Atmospheric Research, Computational and Information Systems Laboratory. Dataset.

Patra P K, Dileep Kumar M, Mahowald N, Sarma V V S S (2007). Atmospheric deposition and surface stratification as controls of contrasting chlorophyll abundance in the North Indian Ocean. J Geophys Res Oceans, 112(C5): C05029

Prasannakumar S, Muraleedharan P M, Prasad T G, Gauns M, Madhupratap M (2002). Why is the Bay of Bengal less productive during summer monsoon compared to the Arabian Sea? Geophys Res Lett, 29(24): 2235

Shafeeque M, Sathyendranath S, George G, Balchand A N, Platt T (2017). Comparison of seasonal cycles of phytoplankton chlorophyll, aerosols, winds and sea-surface temperature off somalia. Front Marine Sci, 4: 386

Singh R P, Prasad A K, Kayetha V K, Kafatos M (2008). Enhancement of oceanic parameters associated with dust storms using satellite data. J Geophys Res Oceans, 113(C11): C11008

Smith S L, Codispoti L A (1980). Southwest monsoon of 1979: chemical and biological response of Somali coastal waters. Science, 209 (4456): 597–600

Tang D L, Kawamura H, Luis A J (2002). Short-term variability of phytoplankton blooms associated with a cold eddy in the north-western Arabian Sea. Remote Sens Environ, 81(1): 82–89

Tindale N W, Pease P P (1999). Aerosols over the Arabian Sea: atmospheric transport pathways and concentrations of dust and sea salt. Deep Sea Res Part II Top Stud Oceanogr, 46(8–9): 1577–1595

Vickers D, Mahrt L, Andreas E L (2013). Estimates of the 10-m neutral sea surface drag coefficient from aircraft eddy-covariance measurements. Phys Oceanogr, 43(2): 301–310

Wessel P, Smith W H F (1996). A global, self-consistent, hierarchical, high-resolution shoreline database. J Geophys Res, 101(B4): 8741–8743

Wiggert J D, Hood R R, Banse K, Kindle J C (2005). Monsoon-driven biogeochemical processes in the Arabian Sea. Prog Oceanogr, 65(2–4): 176–213

Wiggert J D, Murtugudde R G, Christian J R (2006). Annual ecosystem variability in the tropical Indian Ocean: results of a coupled bio-physical ocean general circulation model. Deep Sea Res Part II Top Stud Oceanogr, 53(5–7): 644–676

Wiggert J D, Murtugudde R G (2007). The sensitivity of the southwest monsoon phytoplankton bloom to variations in aeolian iron deposition over the Arabian Sea. J Geophys Res, 112(C5): C05005

Zhao H, Tang D L (2007). Effect of 1998 El Niño on the distribution of phytoplankton in the South China Sea. J Geophys Res, 112: C02017

Zhao H, Wang Y Q (2018). Phytoplankton increases induced by tropical cyclones in the South China Sea during 1998–2015. JGR Oceans, 123(4): 2903–2920

Zhao H, Zhang S P (2014). Review on spatial-temporal variation of China's offshore phytoplankton chlorophyll and primary productivity and their variational mechanism. J Guangdong Ocean Univ, 34 (01): 98–104

Zhao H, Zhao J, Sun X, Chen F, Han G (2018). A strong summer phytoplankton bloom southeast of Vietnam in 2007, a transitional year from El Niño to La Niña. PLoS One, 13(1): e0189926